

The JCMT Nearby Galaxies Legacy Survey I. Star Forming Molecular Gas in Virgo Cluster Spiral Galaxies

C. D. Wilson¹, B. E. Warren¹, F. P. Israel², S. Serjeant³, G. Bendo⁴, E. Brinks⁵, D. Clements⁴, S. Courteau⁶, J. Irwin⁶, J. H. Knapen⁷, J. Leech⁸, H. E. Matthews⁹, S. Mühle¹⁰, A. M. J. Mortier¹¹, G. Petitpas¹², E. Sinukoff¹, K. Spekkens¹³, B. K. Tan⁸, R. P. J. Tilanus^{14,15}, A. Usero^{5,16}, P. van der Werf², T. Wiegert¹⁷, & M. Zhu^{9,14}

¹Department of Physics & Astronomy, McMaster University, Hamilton, Ontario L8S 4M1 Canada; wilson@physics.mcmaster.ca, bwarren@physics.mcmaster.ca, sinukoj@mcmaster.ca

²Sterrewacht Leiden, Leiden University, PO Box 9513, 2300 RA Leiden, The Netherlands ;israel@strw.leidenuniv.nl, pvdwerf@strw.leidenuniv.nl

³Department of Physics & Astronomy, The Open University, Milton Keynes, Mk7 6AA England

⁴Astrophysics Group, Imperial College London, Blackett Laboratory, Prince Consort Road, London SW7 2AZ United Kingdom; g.bendo@imperial.ac.uk, d.clements@imperial.ac.uk

⁵Centre for Astrophysics Research, University of Hertfordshire, College Lane, Hatfield AL10 9AB, United Kingdom; E.Brinks@herts.ac.uk

⁶Department of Physics, Engineering Physics and Astronomy, Queen's University, Kingston, ON, Canada; irwin@astro.queensu.ca, courteau@astro.queensu.ca

⁷Instituto de Astrofísica de Canarias, 38200 La Laguna, Spain; jhk@iac.es

⁸Department of Physics, University of Oxford, Keble Road, Oxford OX1 3RH, UK; jxl@astro.ox.ac.uk

⁹National Research Council Canada, Herzberg Institute of Astrophysics, DRAO, P.O. Box 248, White Lake Road, Penticton, BC V2A 6J9, Canada; henry.matthews@nrc-cnrc.gc.ca

¹⁰Joint Institute for VLBI in Europe, Postbus 2, 7990 AA Dwingeloo, The Netherlands; muehle@jive.nl

¹¹SUPA¹ Institute for Astronomy, University of Edinburgh, Royal Observatory, Blackford Hill, Edinburgh, EH9 3HJ, UK; ajm@roe.ac.uk

¹²Harvard-Smithsonian Center for Astrophysics, Cambridge, MA 02138; gpetitpa@cfa.harvard.edu

¹³Department of Physics, Royal Military College of Canada, PO Box 17000, Station "Forces", Kingston, K7K 4B4 Ontario, Canada; Kristine.Spekkens@rmc.ca

¹⁴Joint Astronomy Centre, 660 N. A'ohoku Pl., Hilo, Hawaii, 96720, USA; r.tilanus@jach.hawaii.edu, m.zhu@jach.hawaii.edu

¹⁵Netherlands Organisation for Scientific Research, The Hague

¹⁶Observatorio Astronómico Nacional, C/ Alfonso XII 3, 28014 Madrid, Spain; a.usero@oan.es

¹⁷Department of Physics and Astronomy, University of Manitoba, Winnipeg, Manitoba R3T 2N2, Canada;

ABSTRACT

We present large-area maps of the CO $J=3-2$ emission obtained at the James Clerk Maxwell Telescope for four spiral galaxies in the Virgo Cluster. We combine these data with published CO $J=1-0$, $24\ \mu\text{m}$, and $\text{H}\alpha$ images to measure the CO line ratios, molecular gas masses, and instantaneous gas depletion times. For three galaxies in our sample (NGC 4254, NGC4321, and NGC 4569), we obtain molecular gas masses of $7 \times 10^8 - 3 \times 10^9 M_{\odot}$ and disk-averaged instantaneous gas depletion times of 1.1-1.7 Gyr. We argue that the CO $J=3-2$ line is a better tracer of the dense star forming molecular gas than the CO $J=1-0$ line, as it shows a better correlation with the star formation rate surface density both within and between galaxies. NGC 4254 appears to have a larger star formation efficiency(smaller gas depletion time), perhaps because it is on its first passage through the Virgo Cluster. NGC 4569 shows a large-scale gradient in the gas properties traced by the CO $J=3-2/J=1-0$ line ratio, which suggests that its interaction with the intracluster medium is affecting the dense star-forming portion of the interstellar medium directly. The fourth galaxy in our sample, NGC 4579, has weak CO $J=3-2$ emission despite having bright $24\ \mu\text{m}$ emission; however, much of the central luminosity in this galaxy may be due to the presence of a central AGN.

Subject headings: galaxies: clusters: individual (Virgo) – galaxies: ISM — galaxies: individual(NGC 4254, NGC 4321, NGC 4569, NGC4579) – galaxies: spiral – ISM: molecules – stars: formation

1. Introduction

Molecular gas provides the fuel for star formation and therefore plays an important role in both the current appearance and future evolution of galaxies. Early surveys for molecular gas in galaxies revealed a wide range in total gas content, from the rarely detected elliptical galaxies to gas-rich massive spirals such as M51 (Young & Scoville 1991; Braine et al. 1993; Young et al. 1995). For spiral galaxies, the variations in gas content roughly track the star

wiegert@physics.umanitoba.ca

¹Scottish Universities Physics Alliance

formation rate for different systems, such that the global star formation efficiency (the inverse of which is the gas depletion time, $t_{gas} = M_{H_2}/SFR$) does not depend strongly on morphology when far-infrared luminosity is used to trace the star formation rate (Young & Scoville 1991). Detailed studies of individual galaxies provided evidence for enhanced star formation efficiencies (implying shorter instantaneous gas depletion times) at certain positions within spiral arms (Vogel et al. 1988) or along them (Knapen et al. 1992, 1996) compared to the disk-averaged value. A focused survey of spiral galaxies in the Virgo cluster showed that the molecular gas content of HI-deficient cluster spirals is similar to that of their more gas-rich counterparts (Kenney & Young 1989). Kennicutt et al. (2007) find that the star formation rate surface density correlates with the molecular but not the atomic gas surface density.

To date, most large surveys of molecular gas in galaxies have been carried out using the CO $J=1-0$ transition; this line is sensitive to the vast majority of molecular gas in the cold interstellar medium in galaxies, since the $J=1$ level is only 5.5 K above the ground state and the $J=1-0$ transition has a critical density of $1.1 \times 10^3 \text{ cm}^{-3}$ in optically thin gas. The detailed connection between CO emission and molecular gas mass and ultimately the star formation process depends rather critically on the value of the CO-to- H_2 conversion factor (Strong et al. 1988) and any dependencies of that conversion factor on temperature, density, or metallicity (Dickman et al. 1985; Maloney & Black 1988). While individual galaxies have been studied in higher transitions, primarily CO $J=2-1$ and CO $J=3-2$, the only large surveys available to date in the CO $J=3-2$ transition are observations of the central regions of galaxies (Mauersberger et al. 1999; Hafok & Stutzki 2003; Yao et al. 2003; Komugi et al. 2007). Since the CO $J=3$ level is 33 K above the ground state and the $J=3-2$ transition has a critical density of $2.1 \times 10^4 \text{ cm}^{-3}$ in optically thin gas, the $J=3-2$ transition naturally traces gas that is on average warmer and/or denser than the CO $J=1-0$ line.

Examining the CO $J=3-2/1-0$ line ratio both within and between galaxies can give information on any large-scale variations in the physical conditions in the molecular gas (Wilson et al. 1997; Petitpas & Wilson 2000). In addition, the CO $J=3-2$ emission may trace the molecular gas that is more directly connected with star formation; indeed, Iono et al. (2008) have found that the global CO $J=3-2$ luminosity correlates nearly linearly with the global star formation rate over five orders of magnitude. Bigiel et al. (2008) also find a nearly linear relation between the H_2 surface density traced by the CO $J=2-1$ line and the star formation rate surface density. These relations are similar to the linear correlation of HCN with far-infrared luminosity seen by Gao & Solomon (2004) and suggests that these CO transitions may also be effective tracers of the densest, star forming gas. In contrast, the CO $J=1-0$ luminosity has a much shallower correlation with star formation rate with a slope 0.62 ± 0.08 (Greve et al. 2005). This shallower slope implies that there is not a one-to-one relation between the amount of molecular gas (as traced by the CO $J=1-0$ line) and

the amount of star formation in a galaxy. The shallower slope compared to the CO $J=3-2$ data also indicates that the two lines are not tracing exactly the same gas components. For example, the CO $J=1-0$ line can include emission from lower opacity, more diffuse molecular gas (Wilson & Walker 1994; Rosolowsky & Blitz 2005). Examining the correlation between molecular gas and star formation rate as a function of the gas density may yield new insights into the star formation process in galaxies.

An ideal laboratory for the acquisition of resolved molecular maps in galaxies is the nearby Virgo Cluster. At a distance of 16.7 Mpc (Mei et al. 2007), it is the largest concentration of galaxies (cluster mass $4.2 \times 10^{14} M_{\odot}$; McLaughlin 1999) within 35 Mpc. It has been the target of numerous studies over the years and plays an important role in our understanding of how galaxies evolve in dense environments. The most extensive optical survey was carried out by Binggeli et al. (1985) and resulted in the Virgo Cluster Catalog (VCC) containing ~ 2100 certain or possible cluster members over an area of 140 deg^2 . The Virgo Cluster is particularly interesting for studying the impact of the dense environment on the ISM in galaxies, as properties such as ram-pressure stripping, tidal interactions, etc., become important in environments with a massive intracluster medium.

Recently, the Virgo Cluster has been included within the area being mapped in the HI 21 cm line by the ALFALFA survey (Giovanelli et al. 2005). Comparison with optical catalogs shows ~ 200 detections associated with optical counterparts as well as 10 detections associated with tidal debris tails (Gavazzi et al. 2008). High-resolution HI observations with the VLA have identified seven spiral galaxies with long HI tails pointing away from M87 (Chung et al. 2007), which suggests that interaction with the cluster as a whole has created these tails. Other evidence for environmental modification includes ram-pressure stripped extraplanar gas tails and disturbances in radio morphologies (Kenney et al. 2008; Murphy et al. 2008).

Spiral galaxies in the Virgo Cluster were first surveyed for molecular emission by Stark et al. (1986), who detected 23 out of 47 spirals observed with a beam size of $100''$. The primary reference for the molecular gas content of spiral galaxies in the Virgo Cluster remains the work of Kenney & Young (1986, 1988a,b, 1989). Using a complete blue-magnitude selected sample, they found that the molecular gas content of HI-deficient cluster spirals in Virgo is similar that of to their more gas-rich counterparts. Interferometric CO $J=1-0$ observations of 15 Virgo galaxies show a wide range of molecular gas morphology as well as higher molecular gas concentrations in the galaxies with deeper gravitational potential wells (Sofue et al. 2003a,b). High resolution CO $J=1-0$ images for a few galaxies in the Virgo cluster are also presented in Helfer et al. (2003) and Kuno et al. (2007). Hafok & Stutzki (2003) made low resolution observations of the CO $J=3-2$ and $J=2-1$ lines with the KOSMA 3 m telescope

of the 20 strongest sources from the CO $J=1-0$ survey of Stark et al. (1986). They detected 18 and 16 spiral galaxies, respectively, in the two lines and measured CO $J=3-2/J=1-0$ line ratios ranging from 0.14 to 0.35 and CO $J=2-1/1-0$ line ratios from 0.5 to 1.1.

The star formation properties of Virgo cluster galaxies have also been studied extensively. Koopmann & Kenney (2004a) found that half of the bright Virgo spirals have truncated $H\alpha$ disks even though they have relatively undisturbed stellar disks. This truncation suggests that ICM-ISM stripping is primarily responsible for the reduced star formation rates of bright Virgo spirals (Gavazzi et al. 2002; Koopmann & Kenney 2004b). Fumagalli & Gavazzi (2008) found that cluster members which have lost even a moderate amount of their atomic gas also have lower molecular gas content and star formation rates.

In this paper, we present some first results from the JCMT Nearby Galaxies Legacy Survey (NGLS). We focus on new, wide-area observations of the CO $J=3-2$ emission for the four large spiral galaxies in the Virgo Cluster (NGC 4254, NGC 4321, NGC 4569, and NGC 4579) that are part of the Spitzer Infrared Nearby Galaxies Survey (SINGS) sample (Kennicutt et al. 2003). We briefly describe the structure and goals of the NGLS in §1.1 and review previous observations of the interstellar medium in the particular Virgo Cluster galaxies in our sample in §1.2. We discuss our observations and data reduction in §2. In §3, we combine the data with CO $J=1-0$ maps from Kuno et al. (2007) to estimate the CO $J=3-2/J=1-0$ line ratio and the molecular gas mass. In §4, we combine these new data with $H\alpha$ data and reprocessed 24 μm data from the SINGS survey (Kennicutt et al. 2003) to obtain maps of the star formation rate (Calzetti et al. 2007) and gas depletion time. We discuss the usefulness of the CO $J=3-2$ line as a tracer for dense star forming gas and the gas and star formation properties of the four galaxies in the context of their internal structure and broader environment in §5. We give our conclusions in §6.

1.1. The JCMT Nearby Galaxies Legacy Survey

The JCMT Nearby Galaxies Legacy Survey (NGLS)² focuses on the molecular gas and dust content of galaxies within 25 Mpc using three primary samples: (1) galaxies from the SINGS (Kennicutt et al. 2003) sample (see B. E. Warren et al. 2009, for first results from the NGLS for additional SINGS galaxies); (2) an HI flux limited sample of galaxies from the Virgo cluster; and (3) an HI flux limited sample of galaxies in the field. The first phase of the NGLS consists of CO $J=3-2$ observations out to $D_{25}/2$ for 21 galaxies from the SINGS sample as well as the complete Virgo sample; this phase of the survey is currently complete.

²<http://www.jach.hawaii.edu/JCMT/surveys/>

The second phase consists of CO $J=3-2$ observations for the entire sample and will begin in 2009 if additional observing time is allocated to the survey. The third phase, for which observing time has been allocated already, will consist of SCUBA-2 observations of the entire sample and should begin in late 2009.

Specific science goals for the NGLS include: searching for evidence of cold dust and measuring its mass fraction in galaxies of different types; measuring the amount of warm, dense molecular gas associated with star formation using the CO $J=3-2$ line; comparing galaxies with similar morphologies and luminosities in the field and in the Virgo cluster to determine the effects of cluster membership; using CO rotation curves to trace the dark matter distribution and the frequency of occurrence of nuclear gas concentrations which may feed central starbursts or black holes; and measuring the local submillimeter luminosity function and dust mass function to luminosities up to 100 times fainter than previous studies (e.g., Dunne et al. 2000).

1.2. Properties of four Virgo spiral galaxies

Four large spiral galaxies (NGC 4254, NGC 4321, NGC 4569, and NGC 4579) are the only Virgo Cluster galaxies included in the SINGS survey (Kennicutt et al. 2003) and there is a large collection of information on their dust and interstellar medium properties. Some basic properties of the galaxies are given in Table 1. The global 1-850 μm spectral energy distributions (SEDs) for these four galaxies are very similar (Dale et al. 2005), although the α parameter in the SED fit ranges from a high 3.8 in NGC 4579 to a low of 2.4 in NGC 4254. Draine et al. (2007) calculate the dust mass and gas to dust ratio for 65 galaxies in the SINGS sample. Of the four Virgo spirals discussed in our paper, only NGC 4579 stands out as having a factor of 3 larger gas to dust ratio; this is the second highest gas to dust ratio in the entire sample analyzed by Draine et al. (2007). This high gas-to-dust ratio may be a by-product of the difficulty in determining the 850 μm flux from the relatively low signal-to-noise SCUBA map (Bendo, private communication). Morphologically, of the four Virgo spirals, NGC 4569 is the most centrally concentrated at 24 μm , while NGC 4254 is both the least centrally concentrated and the most asymmetric (Bendo et al. 2007). The star formation distribution based on $\text{H}\alpha$ emission is classified as normal for NGC 4254 but truncated/normal for the other three galaxies (Koopmann & Kenney 2004a). Below we give some important details on each of the individual galaxies.

Recent HI observations of NGC4254 (M99) show a long tidal tail extending to the north; its lopsided morphology, high HI content, and high relative velocity suggest that this galaxy is undergoing its first encounter with the center of the Virgo cluster (Haynes et al. 2007).

The galaxy has a normal molecular gas to total gas fraction (Nakanishi et al. 2006).

NGC 4321 (M100) is classified as HII/LINER (Ho et al. 1997). High resolution CO $J=1-0$ observations show two spiral arms and gas in the nucleus as well as faint emission bridging the arms and the nucleus (García-Burillo et al. 2005). The HI emission is truncated near the edge of the optical disk (Cayatte et al. 1990; Braun et al. 2007). NGC 4321 is interacting with NGC 4322, as shown by the bridge between them that is visible in optical light but not in HI (Knapen et al. 1993). It also has a rather prominent circumnuclear ring with much enhanced star formation (Knapen et al. 1995a,b).

NGC 4569 (M90) has been called an anemic spiral because of the small extent of its HI emission relative to its optical size (Sakamoto et al. 1999), although Koopmann & Kenney (2004a) prefer a designation of truncated/normal because its star formation rate per unit area is relatively normal. Bendo et al. (2007) note that there is almost no $24 \mu\text{m}$ emission from the extended disk. The CO $J=1-0$ emission shows a compact bar oriented roughly north-south (Sakamoto et al. 1999) with complex kinematics indicating non-circular motions in the central arcminute (Jogee et al. 2005). This galaxy has a higher molecular gas to total gas fraction than NGC 4254, perhaps due to ram pressure stripping of HI even within the stellar disk or a higher external pressure due to the intracluster medium (Nakanishi et al. 2006). However, the fact that the only remaining gas is in the inner disk, which tends to have a high molecular gas fraction, could also explain this result. Koopmann & Kenney (2004a) find that the galaxy has some HII regions that appear to be outside the plane. They also note that rotation plus forward motion relative to the ICM can create an asymmetric ram pressure, which in simulations can produce a dominant extraplanar gas arm emerging from a truncated gas disk. Vollmer et al. (2004) present also evidence for ram pressure stripping by comparing the kinematically distinct western arm with dynamical simulations. Boselli et al. (2006) argue that active gas stripping, rather than simply stopping gas inflow, is required to explain the star formation history in NGC 4569. Jogee et al. (2005) suggest that NGC 4569 is in the early stages of bar or tidally driven gas inflow.

NGC 4579 (M58) is classified as LINER 1.9/Seyfert 1.9 (García-Burillo et al. 2005). High resolution CO $J=2-1$ observations show two spiral arms approaching to within a few arcseconds of the AGN (García-Burillo et al. 2005) and weak CO emission at the AGN itself (García-Burillo et al. 2008). At lower resolution, weak CO emission is detected throughout the disk (Nakanishi et al. 2006). Despite the weak emission, this galaxy has a higher molecular gas to total gas fraction than NGC 4254, and so may also have been affected by ram pressure stripping or a higher external pressure (Nakanishi et al. 2006).

In summary, this small sample of four spiral galaxies probes a large fraction of the characteristics seen for luminous spirals in the Virgo cluster such as HI deficiency, star

formation rate, and presence of nuclear activity. Thus, a detailed study of the molecular gas and star formation properties of these galaxies should provide insight into the effects on the ISM in galaxies and galaxy structure and evolution that can be addressed using the complete Virgo sample from the NGLS.

2. Observations and Data Processing

2.1. CO $J=3-2$ Data

The CO $J=3-2$ observations were obtained as part of the JCMT Nearby Galaxies Legacy Survey (NGLS). We used the 16 pixel array receiver HARP-B with the ACSIS correlator configured to have a bandwidth of 1 GHz and a resolution of 0.488 MHz (0.43 km s^{-1} at the frequency of the CO $J=3-2$ transition). The galaxies were observed in raster mapping mode to cover a rectangular area corresponding to $D_{25}/2$ with a 1 sigma sensitivity of better than 19 mK (T_A^*) at a spectral resolution of 20 km s^{-1} . The angular resolution of the JCMT at this frequency is $14.5''$ and the images were processed using $7.2761''$ pixels (the recommended pixel size in the reconstruction of HARP raster maps). Details of the observations are given in Table 2.

Details of the reduction of the CO $J=3-2$ data are given in B. E. Warren et al. (2009) and so we give only a brief summary here. The individual raw data files were flagged to remove data from any of the 16 individual receptors with bad baselines and then the scans were combined into a data cube using a $\text{sinc}(\pi x)\text{sinc}(k\pi x)$ kernel as the weighting function to determine the contribution of individual receptors to each pixel in the final map. A mask was created to identify line-free regions of the data cube and a third-order baseline was fit to those line-free regions. The clumpfind algorithm (Williams et al. 1994) implemented as part of the Starlink/cupid³ task findclumps was used to identify regions with emission above three times the rms noise in a data cube that had been boxcar smoothed by 3 pixels and 25 velocity channels. Moment maps were created from the original data cube using the mask created by findclumps. The data were converted to the main beam temperature scale by dividing by $\eta_{MB} = 0.67$. Maps of the CO $J=3-2$ integrated intensity are given in Figure 1 and are overlaid on images from the Digitized Sky Survey in Figure 2.

³Cupid and kappa are part of the Starlink software package, which is available for download from <http://www.jach.hawaii.edu>

2.2. Ancillary data

The CO $J=1-0$ first moment maps from Kuno et al. (2007) were downloaded from their survey web site. These CO $J=1-0$ data are already in the T_{mb} temperature scale. The angular resolution of the JCMT in the CO $J=3-2$ line closely matches that of the Nobeyama 45 m telescope in the CO $J=1-0$ line. Thus, no additional smoothing was applied.

For comparison with the maps from Kuno et al. (2007), the CO $J=1-0$ first moment maps from Helfer et al. (2003) were downloaded from the NCSA Astronomy Digital Image Library; there was no CO $J=1-0$ image for NGC 4254. The image for NGC 4579 did not include any single dish (short-spacing) data (Helfer et al. 2003) and so must be considered a lower limit to the total CO $J=1-0$ intensity. Each image was convolved with the appropriate two-dimensional gaussian to give a smoothed image with a $14.5''$ circular gaussian beam to match the JCMT resolution and converted from $\text{Jy beam}^{-1} \text{ km s}^{-1}$ to K km s^{-1} using a conversion factor of 0.438 K Jy^{-1} .

The $24 \mu\text{m}$ data from the SINGS survey were reprocessed using an updated version of the data reduction description given in the SINGS Fourth Data Delivery User’s Guide (SINGS team 2006) with three modifications. First, a background offset related to the scan mirror position has been measured and removed from the data. Second, asteroids have been identified and removed from the data. Third, the updated flux calibration terms given by Engelbracht et al. (2007) have been applied to the data. To compare the $24 \mu\text{m}$ images to the JCMT data, we convolved the $24 \mu\text{m}$ images with special convolution kernels that match the profiles of the PSF to the $14.5''$ gaussian function that describes the JCMT beam. These convolution kernels were created using the empirical $24 \mu\text{m}$ PSF described by Young et al. (2009) and the prescription given by Gordon et al. (2008).

The $\text{H}\alpha$ images were downloaded from the SINGS website⁴ (Kennicutt et al. 2003); there was no image for NGC 4569, so we used the image from the GOLD Mine Database (Gavazzi et al. 2003). Although the images were background subtracted, a weakly varying background across the image affected the flux levels once the images were convolved to match the JCMT resolution. We therefore binned the image by 100 pixels and clipped any data above 2 sigma to remove real emission, and then fit a two-dimensional first-order polynomial to the resulting image. The data were calibrated as described in the SINGS release notes. The images were corrected for contamination by the two [NII] lines using the [NII]/ $\text{H}\alpha$ ratios from Prescott et al. (2007). Finally, we convolved the images with a $14.5''$ gaussian to match the resolution of the JCMT.

⁴<http://sings.stsci.edu>

All ancillary data images were aligned with JCMT image orientation and pixel size using the kappa command `wcsalign`. We calculated an image of the star formation rate surface density for each galaxy by combining the $H\alpha$ and $24\ \mu\text{m}$ images using the formula in Calzetti et al. (2007). Maps of the star formation rate for each galaxy are given in Figure 3. For NGC 4579, the central AGN dominates the emission at both $H\alpha$ and $24\ \mu\text{m}$. Thus, Figure 3 does not provide an accurate measure of the star formation rate in the central regions of NGC 4579.

3. CO $J=3-2/J=1-0$ line ratios and molecular gas mass

3.1. CO $J=3-2/J=1-0$ line ratios

All calibrations to date of the conversion from CO luminosity to molecular gas mass have been for the ground state $J=1-0$ transition (Strong et al. 1988). Thus, the CO $J=3-2/J=1-0$ line ratio is an important quantity to measure in determining molecular gas masses. In addition, the CO $J=3-2/J=2-1$ line ratio has been suggested previously to be a good indicator of temperature in giant molecular clouds, with larger ratios corresponding to larger temperatures (Wilson et al. 1997). If the CO $J=2-1/1-0$ line ratio is relatively uniform (Leroy et al. 2008), then the CO $J=3-2/J=1-0$ line ratio would also be a good temperature indicator. Alternatively, the line ratio can be increased if the average density of the gas is increased (see e.g., Petitpas & Wilson 2000, for a discussion of this effect in M82).

High resolution CO $J=1-0$ images for NGC 4321 and NGC 4569 have been published by Helfer et al. (2003) and Kuno et al. (2007). The total CO $J=1-0$ fluxes measured directly from these publicly available integrated intensity maps agree to better than 5%. However, a comparison of the two images pixel by pixel shows systematic differences between the two data sets. In particular, the images from Helfer et al. (2003), which are produced by combining interferometric and single dish data, yield higher intensities around bright and more compact structures compared to the images from Kuno et al. (2007). As such systematic differences could have been produced in the combination of the single dish and interferometric data (which is a tricky and non-linear process), we have chosen to calculate the CO $J=3-2/J=1-0$ line ratios using the data from Kuno et al. (2007). Images of the line ratios are shown in Figure 4. In calculating the average values for each galaxy and for regions within each galaxy, we limited our analysis to pixels with a signal-to-noise in the CO $J=3-2$ line greater than 3. Global and central values for the line ratios as well as line ratios for particular emission peaks within the disk are given in Table 3.

NGC 4254 has a remarkably uniform CO $J=3-2/1-0$ ratio of 0.33. NGC 4321 has a

similar disk-averaged CO $J=3-2/1-0$ ratio of 0.36; however, the average value in the central 9 pixels ($22''$ diameter) is significantly larger at 0.79. NGC 4569 shows a significant gradient from north to south in its line ratio, from 0.53 at the northern CO $J=3-2$ peak to just 0.06 at the southern peak. Its disk averaged value of 0.25 is somewhat lower than the other two galaxies. Finally, NGC 4579 is a difficult case. It is detected weakly by Kuno et al. (2007) but is only marginally detected at CO $J=3-2$ (Fig. 1). Our marginal detection near the star formation peak in the disk is 0.9 ± 0.3 K km s $^{-1}$, while Kuno et al. (2007) detect CO $J=1-0$ emission of 6 K km s $^{-1}$. Combining these two values suggests that the CO $J=3-2/J=1-0$ line ratio in the disk of NGC 4579 is similar to the low line ratio seen in the southern portion of NGC 4569.

Assuming a 15% absolute calibration uncertainty for both CO data sets (§2), the mean line ratios in the three galaxies with good CO $J=3-2$ detections agree at the 1 sigma level. However, the southern half of NGC 4569 has a significantly lower line ratio while the central region of NGC 4321 and the northern emission peak of NGC 4569 have significantly higher line ratios. These line ratios suggest that the gas may be on average somewhat warmer and/or denser in the center of NGC 4321 and north of NGC 4569, while the southern disk of NGC 4569 may be somewhat cooler or less dense than typical disk regions. An intriguing possibility is that the gradient in gas properties in NGC 4569 is related to its interaction with the ICM; we discuss this possibility in §5 below.

The average CO $J=3-2/1-0$ line ratios in these three galaxies are somewhat smaller than the range of values (0.4-0.8) seen in individual giant molecular clouds in M33 (Thornley & Wilson 1994; Wilson et al. 1997). The line ratios do fall within the range of ratios (0.2-0.7) measured with similar angular resolution by Mauersberger et al. (1999), albeit at the low end of the range. However, Mauersberger et al. (1999) observed only the central $21''$ of each galaxy in their sample. If many galaxies have enhanced line ratios in the central region, as we see in NGC 4321 and possibly in NGC 4569, this focus on the central regions could explain their somewhat higher line ratios. Our line ratio for NGC 4569 is in reasonable agreement with the lower-resolution results from Hafok & Stutzki (2003), who measured a line ratio of 0.23 ± 0.04 . However, our line ratios for the other two galaxies are substantially larger than the values measured by them: 0.21 ± 0.04 for NGC 4254 and 0.24 ± 0.02 for NGC 4321. Applying a 3σ clip to the CO $J=3-2$ data has had the effect of limiting our line ratio analysis in these galaxies to brighter regions; for example, the inter-arm regions of NGC 4321 are not detected at this level. If the interarm gas has a substantially lower line ratio, this could explain the difference between our values and those obtained by Hafok & Stutzki (2003).

3.2. Molecular gas mass

The CO $J=3-2$ luminosities and molecular hydrogen gas masses are given in Table 4. Values for the center of NGC 4579 are calculated using a 3σ upper limit and a gaussian line with full-width half-maximum of 200 km s^{-1} . We give two different estimates for the molecular gas mass. The first value is calculated directly from the CO $J=3-2$ luminosity assuming a CO $J=3-2/1-0$ line ratio of 0.6 and adopting a CO to H_2 conversion factor of $2 \times 10^{20} \text{ cm}^{-2} (\text{K km s}^{-1})^{-1}$ (Strong et al. 1988). The CO $J=3-2/1-0$ line ratio of 0.6 is adopted as a typical ratio appropriate to the gas in giant molecular clouds. It is based on observations of an average CO $J=2-1/1-0$ ratio of 0.8 in spiral disks (Leroy et al. 2008) combined with the average CO $J=3-2/J=2-1$ ratio of 0.76 ± 0.19 measured in the Galactic molecular cloud M17 (Wilson et al. 1999). A similar line ratio (0.60 ± 0.13) is observed in the central regions of 15 nearby galaxies with modest starbursts (Israel 2008, 2009). Adopting a line ratio specifically appropriate for molecular clouds essentially uses the CO $J=3-2$ emission to focus in on the star forming molecular gas; the CO $J=1-0$ line has been shown to include emission from lower opacity, more diffuse molecular gas (Wilson & Walker 1994; Rosolowsky & Blitz 2005) which likely does not participate directly in massive star formation.

Alternatively, we could adopt the average CO $J=3-2/J=1-0$ line ratio measured in our sample, which is 0.34 averaged over the three galaxies in our sample. This mass estimate essentially measures the total molecular hydrogen content and should be directly comparable (modulo issues of area coverage and sensitivity) to previous estimates of the molecular gas mass derived directly from CO $J=1-0$ maps. Table 4 also gives masses measured directly from the data of Kuno et al. (2007) as well as the masses estimated by Helfer et al. (2003) from their single-dish maps. For NGC 4254 and NGC 4321, the CO $J=1-0$ masses from Kuno et al. (2007) are in general agreement with the masses calculated from the CO $J=3-2$ line when the line ratio of 0.34 is adopted, as expected given the quite uniform line ratio seen in these galaxies. However, for NGC 4569, the CO $J=1-0$ mass is almost a factor of three times larger than the CO $J=3-2$ mass. This larger mass is partly a result of the fact that the CO $J=3-2/J=1-0$ ratio in this galaxy is the lowest of the three (accounting for a factor of 1.4 in mass) and also that the southern region of the galaxy is quite bright in CO $J=1-0$ but almost invisible in CO $J=3-2$. For NGC 4579, the CO $J=1-0$ mass is a factor of ten larger than the upper limit to the CO $J=3-2$ mass, again consistent with the very weak CO $J=3-2$ emission in this galaxy as a whole.

How are we to understand the variety of gas masses given in Table 4? The most straightforward interpretation is that the gas mass calculated from the CO $J=3-2$ luminosity using a CO $J=3-2/J=1-0$ line ratio of 0.6 (as seen in Galactic GMCs) traces the dense

molecular gas, while the mass calculated directly from the CO $J=1-0$ luminosity traces the total molecular gas mass. With this interpretation, the dense gas fraction in the galaxies in our sample is 46% for NGC 4254, 65% for NGC 4321, 22% for NGC 4569, and <7% for NGC 4579. However, this simple picture is muddled by the disagreement between the CO $J=1-0$ data of Helfer et al. (2003) and Kuno et al. (2007). Although the total fluxes in the published CO $J=1-0$ integrated intensity images for NGC 4321 and NGC 4569 are very similar, the *total* mass from the single-dish maps of Helfer et al. (2003) is a factor of 2 larger in NGC 4321 and a factor of 0.8 smaller in NGC 4569, such that the dense gas fraction in the two galaxies becomes quite similar if we use the masses from Helfer et al. (2003). While some of these variations may be attributed to such factors as calibration uncertainties (to explain NGC 4569) and larger mapping area (for NGC 4321), the fact remains that considerable uncertainties, perhaps as large as a factor of two, continue to plague these gas mass estimates.

4. Gas depletion times

The instantaneous gas depletion time (t_{gas}) can be calculated as the ratio of the molecular gas mass divided by the star formation rate. The inverse of the gas depletion time is often referred to as the star formation efficiency (Young & Scoville 1991). In this section, we examine the gas depletion times both within and between the galaxies in our sample. We focus first on the gas depletion time calculated assuming a CO $J=3-2/J=1-0$ ratio of 0.6, which is essentially a depletion time for the dense gas. In the next section, we compare these gas depletion times to values obtained using the CO $J=1-0$ line. Note that the *instantaneous* gas depletion time (or star formation efficiency) traces the rate at which currently available molecular gas is being turned into stars, and will give (often substantially) shorter times than global gas depletion times calculated from the total gas reservoir (molecular plus atomic gas). In the calculations of gas depletion time, we include a factor of 1.36 to take into account the mass contribution of helium.

We made maps of t_{gas} for NGC4254, NGC 4321, and NGC 4569 by combining the star formation rate maps described in §2 with CO $J=3-2$ integrated intensity maps containing only pixels detected at the 3σ level or above. We assume a CO line ratio of 0.6 and adopt a CO to H₂ conversion factor of $2 \times 10^{20} \text{ cm}^{-2} (\text{K km s}^{-1})^{-1}$ (Strong et al. 1988). Maps of the gas depletion time are given in Figure 5, where the units of t_{gas} are Gyr. Global and central values for the gas depletion times as well as values for emission peaks within the disk are given in Table 5.

For NGC 4254, the average value of t_{gas} is 1.1 Gyr. For NGC 4321, the average value

of t_{gas} is 1.7 Gyr, while for NGC 4569 it is 1.6 Gyr, both values 50% larger than the gas depletion time for NGC 4254. The gas depletion times show the most variation in NGC 4569, but are still quite uniform across the disk. The value in the central region (0.9 Gyr) is about half the average value in the disk. The value measured at the peak of the CO emission in the southern half of the galaxy is somewhat lower still at 0.6 Gyr, while the value at the northern CO peak is closer to the disk mean value at 1.2 Gyr. Note that the weak CO $J=3-2$ emission in the southern half of the galaxy is balanced by the lower star formation rate to give a similar gas depletion time. For NGC 4579, the nominal gas depletion time for the one pixel to the west of the nucleus where the weak CO emission aligns with a region of star formation is 0.25 Gyr, a factor of four smaller than the average gas depletion time in NGC 4254 and a factor of six smaller than the gas depletion times for NGC 4321 and NGC 4569. Because of the strong AGN in NGC 4579 (see §5), we cannot obtain a reliable estimate of the gas depletion time in the nucleus from our analysis.

Thus, of the three galaxies in our sample with strong CO $J=3-2$ emission, NGC 4254, which has a normal HI content for its type, has a smaller gas depletion time by a factor of 1.5 compared to NGC 4321 and NGC 4569. These two galaxies have very similar instantaneous depletion times for the dense gas, despite having a factor of three difference in their HI deficiency (Table 1). The gas depletion times in these three galaxies comparable to or somewhat smaller than the values of $\sim 2 \times 10^9$ yr obtained in spiral galaxies by Leroy et al. (2008) and Bigiel et al. (2008). Overall, the gas depletion times calculated here are significantly smaller than a Hubble time. One reason is that we are calculating an instantaneous gas depletion time by focusing just on the dense molecular component rather than including the entire gas reservoir (atomic plus all phases of molecular gas at all radii). Radial infall of gas from the outer atomic disks can provide new fuel for star formation; however, this process is likely to be less effective in cluster galaxies where the outer disk has been removed (Larson et al. 1980). Another reason that these numbers should not be taken as evidence that these Virgo spirals will imminently “run out” of gas to fuel star formation is that we have not attempted to include the effect of return of material to the ISM via supernovae, stellar winds, and stellar evolution. These gas depletion times provide a useful snapshot of the current rate at which gas is being turned into stars, in the same way that the $H\alpha$ and $24 \mu\text{m}$ emission captures the formation of massive ($> 10 M_{\odot}$) stars over the last 10-20 Myr.

5. The broader implications for molecular gas and star formation

5.1. The effects of internal structure and external environment

How do the variations in the gas and star formation properties of these four galaxies relate to their internal structure and larger environment? NGC 4254 has been suggested to be on its first encounter with the central regions of the cluster and, indeed, has a normal ratio of molecular to atomic gas and a normal extent of star formation. It is also the only galaxy in our sample that does not show evidence of a bar (Laine et al. 2002). Its smaller gas depletion time translates into a higher current star formation efficiency; this higher efficiency may be due to the fact that the galaxy has only begun to be disturbed by the cluster (e.g., Haynes et al. 2007).

NGC 4321 is classified as weakly barred (SAB(s)bc, Buta et al. 2007); high resolution CO $J=1-0$ observations show two spiral arms and gas in the nucleus as well as faint emission bridging the arms and the nucleus (García-Burillo et al. 2005). There is also a prominent circumnuclear ring with enhanced star formation (Knapen et al. 1995a,b). Thus, the similar gas depletion times calculated for the central region and the spiral arms suggests that increased star formation is balanced by an increased molecular gas content in these regions.

For NGC 4569, the somewhat lower CO $J=3-2/J=1-0$ ratio of 0.25 suggests that the average gas in NGC 4569 may be somewhat cooler and/or less dense than the gas in NGC 4254 or 4321. However, this potential difference in average gas properties does not seem to have a strong effect on the gas depletion time (or star formation efficiency) estimated using the CO $J=3-2$ line. Given the nearly edge-on orientation of NGC 4569, it is possible that the contribution from CO $J=1-0$ emission in the outer disk of the galaxy contributes significantly to the measured line ratio, while the CO $J=3-2$ is confined to the inner disk regions along with the star formation. NGC 4569 is the largest of the Virgo spirals in our sample, yet its CO $J=3-2$ emission is the most compact. This morphology suggests that whatever processes are acting to strip the outer portions of the galaxy of gas are also affecting the distribution of the dense molecular gas, perhaps by stripping it directly or by removing the reservoir (atomic hydrogen or diffuse molecular hydrogen) from which it forms. The southern portion of the galaxy contains much less dense molecular gas and star formation than the northern half. Given the geometry of the galaxy (Vollmer et al. 2004), the northern portion seems likely to be more affected by interaction with the IGM as its rotational motion and motion through the cluster are in the same sense. The higher density or warmer gas in the northern half of NGC 4569 could possibly be due to gas compression in this region where ram pressure is active.

NGC 4579 appears to be the most unusual galaxy of our small sample. Its disk has

the smallest gas depletion time (highest star formation efficiency) of any of the four galaxies in our sample. The relatively weaker star formation in this galaxy as well as its more limited spatial extent (Figure 3) suggests a galaxy which may be exhausting its fuel for star formation. Its relatively early morphological type (SAB(rs)ab, Buta et al. 2007) is consistent with this picture, although NGC 4569 has an identical classification. However, the higher inclination of NGC 4569 means that a given surface density of molecular gas is more easily detected than in NGC 4579. Indeed, the relatively weak CO $J=3-2$ emission in the southern half of NGC 4569 would be undetectable if it were at the same inclination as NGC 4579. In addition, the broader lines (full-width zero intensity 400-500 km s^{-1}) seen in the central region of NGC 4579 by (García-Burillo et al. 2008) also imply that its central CO emission is harder to detect than the central emission in NGC 4569. Thus, NGC 4579 may not be such an unusual galaxy for its type, but simply observed at a less favorable inclination angle than NGC 4569.

5.2. Which CO transition traces star forming gas best?

In §4, we calculated gas depletion times by combining directly the CO $J=3-2$ intensity with the star formation rate. If instead we use the CO $J=1-0$ intensity from Kuno et al. (2007), and study exactly the same regions in each galaxy as in §4, the picture becomes more complicated. Values for the gas depletion time calculated using the CO $J=1-0$ line are also given in Table 5.

For NGC 4254, the gas depletion times remain very uniform when the CO $J=1-0$ line is used instead of the $J=3-2$ line to trace the molecular gas. The average gas depletion time shows a larger dispersion, which hints at more local variations than are seen using the CO $J=3-2$ line; however, this could also be due to low signal-to-noise CO $J=1-0$ spectra being included in our analysis.

For NGC 4321, when the CO $J=1-0$ line is used, the line ratio is also quite uniform overall but the gas depletion time for the central region is now roughly twice as small as that of the disk. The gas depletion times in the CO peaks associated with the spiral arms are intermediate between these two extremes. The disk-averaged gas depletion time remains about 50% larger than that of NGC 4254 whether the CO $J=1-0$ or $J=3-2$ transition is used to trace the molecular gas.

For NGC 4569, the gas depletion times now show significant variations, ranging from 9.0 Gyr at the southern CO $J=3-2$ peak to 1.8 Gyr for the central region. The disk averaged value of 5.4 Gyr, with its larger relative dispersion, also suggests more variation in the gas

depletion time derived from the CO $J=1-0$ line, and is now almost 3 times larger than the gas depletion time in NGC 4254.

Thus, for these three galaxies, using the CO $J=1-0$ line to calculate the gas depletion time instead of the $J=3-2$ line results in a greater spread in gas depletion times both within galaxies and from one galaxy to another. If we assume that the star formation efficiency (and hence gas depletion time) should not vary significantly from one normal spiral galaxy to another, then this analysis suggests that the CO $J=3-2$ line may be a more direct tracer of the dense, star forming molecular gas than is the CO $J=1-0$ line. This result is consistent with the analysis of Iono et al. (2008), who find a nearly linear correlation between the CO $J=3-2$ luminosity and the far-infrared luminosity (as a tracer of star formation) over 5 orders of magnitude in galaxy luminosity. The good correlation between the star formation rate surface density and the CO $J=3-2$ emission suggests that the CO $J=3-2$ transition probes sufficiently high gas densities to be a good tracer of the dense cores within molecular clouds that are forming stars with a high efficiency. In contrast, the CO $J=1-0$ line traces gas with a wider range of densities, including more diffuse material that is not directly involved in star formation. In this interpretation, using the CO $J=3-2$ line results in a more accurate measurement of the instantaneous gas depletion time.

An alternative interpretation would be that the star forming molecular gas (and the gas depletion time) is in fact well-traced by the CO $J=1-0$ line, and the variations seen both within and between galaxies are real. In this case, regions with higher star formation efficiencies (or smaller gas depletion times) would be those with a higher rate of energy injected due to recent star formation per unit mass of molecular gas. This higher rate of energy injection could warm the molecular gas, producing brighter CO $J=3-2$ emission and leading to a more uniform apparent gas depletion times when the CO $J=3-2$ emission line is used, as observed. While such heating processes are undoubtedly at work in the ISM, we argue that the interpretation of the CO $J=3-2$ line as a direct tracer of dense star-forming gas is the more straightforward explanation.

6. Conclusions

We have used the JCMT to map the CO $J=3-2$ emission from four spiral galaxies in the Virgo cluster. These galaxies are included in the SINGS survey (Kennicutt et al. 2003) and so have a wealth of information on their dust and interstellar medium properties. These galaxies also allow us to probe a range of galaxy properties including HI deficiency, star formation rate, and nuclear activity.

Bright CO $J=3-2$ emission is detected over the extended disks of NGC 4254, NGC4321, and NGC 4569; NGC 4579 is weakly detected (3σ) at one position in the disk and has only an upper limit in the central region. Combining our data with CO $J=1-0$ maps from Kuno et al. (2007), we derive disk-averaged CO $J=3-2/J=1-0$ line ratios of 0.33 in NGC 4254, 0.36 in NGC 4321, and 0.25 in NGC 4569. The line ratio in the center of NGC 4321 is significantly larger (0.79), while NGC 4569 shows a gradient in the line ratio from 0.06 in the south to 0.53 in the north. The very weak CO $J=3-2$ emission in NGC 4579 suggests a line ratio in the disk similar to the lowest value seen in NGC 4569. These line ratios are towards the low end of the range typically measured in galaxies (Mauersberger et al. 1999). However, previous observations have focused on the extreme central regions, which our data suggest may have enhanced line ratios in many galaxies.

We combine $H\alpha$ and $24\ \mu\text{m}$ images from the SINGS survey (Kennicutt et al. 2003) to obtain maps of the star formation rate following the prescription in Calzetti et al. (2007). We combine these star formation rate images with maps of the molecular gas surface density derived from the CO $J=3-2$ data to obtain maps of the instantaneous gas depletion timescale (the inverse of the star formation efficiency). Of the three CO-bright galaxies, the disk-averaged gas depletion time is shortest for NGC 4254 (1.1 Gyr), roughly 50% less than for NGC 4321 (1.7 Gyr) and NGC 4569 (1.6 Gyr). The fourth galaxy, NGC 4579, has weak CO $J=3-2$ emission and small gas depletion times in the disk, 4-6 times smaller than in the other three galaxies. These times, which are substantially shorter than a Hubble time, are a measure of the instantaneous gas depletion time and do not take into account possible replenishing of the dense molecular gas from more diffuse molecular or atomic gas.

We have compared the gas depletion times obtained using the CO $J=3-2$ emission with those obtained using the CO $J=1-0$ emission, which is the more commonly used tracer of molecular gas. We find that using the CO $J=3-2$ line results in more uniform instantaneous gas depletion times both within galaxies and from one galaxy to another. We argue that the CO $J=3-2$ line is a better tracer of the dense molecular gas involved in star formation than the CO $J=1-0$ line. Alternatively, real variations in the star formation efficiency may result in variation in the amount of heating per unit gas, leading to more uniform apparent gas depletion times using the CO $J=3-2$ line. These two scenarios may be testable using radiative transfer codes and multiple CO emission lines to measure the average physical conditions in the molecular gas.

Looking at the internal structure and external environment, we suggest that the smaller gas depletion time (or larger star formation efficiency) in NGC 4254 may be due to the fact that it seems to be encountering the dense portion of the Virgo cluster for the first time (Haynes et al. 2007). In NGC 4569, the gradient in the CO $J=3-2/J=1-0$ line ratio (and

more weakly in the gas depletion time) from south to north suggests that active ram pressure in the northern half of the galaxy may be producing an increase in the average density or temperature of the molecular gas.

We thank the anonymous referee for a very useful referee report. The James Clerk Maxwell Telescope is operated by The Joint Astronomy Centre on behalf of the Science and Technology Facilities Council of the United Kingdom, the Netherlands Organisation for Scientific Research, and the National Research Council of Canada. The research of J.I., S.C., K.S., and C.D.W. is supported by grants from NSERC (Canada). A.U. has been supported through a Post Doctoral Research Assistantship from the UK Science & Technology Facilities Council. This research has made use of the GOLD Mine Database. We acknowledge the usage of the HyperLeda database (<http://leda.univ-lyon1.fr>).

Facilities: JCMT.

REFERENCES

- Bendo, G. J. et al. 2007, MNRAS, 380, 1313
- Bigiel, F., Leroy, A. K., Walter, F., Brinks, E., de Blok, W. J. G., Madore, B., & Thornley, M. D., 2008, AJ, in press (arXiv:0810.2541)
- Binggeli, B., Sandage, A., & Tammann, G., 1985, AJ, 90, 1681
- Boselli, A., Boissier, S., Cortese, L., Gil de Paz, A., Seibert, M., Madore, B. F., Buat, V., & Martin, D. C., 2006, ApJ, 651, 811
- Braine, J., Combes, F., van Driel, W., 1993, A&A, 280, 451
- Braun, R., Oosterloo, T. A., Morganti, R., Klein, U., & Beck, R., 2007, A&A, 461, 455
- Buta, R. J., Corwin, H. G., Odewahn, S. C. 2007, The de Vaucouleurs Atlas of Galaxies (Cambridge: Cambridge University Press)
- Calzetti, D. et al. 2007, ApJ, 666, 870
- Cayatte, V., van Gorkom, J. H., Balkowski, C., & Kotanyi, C. 1990, AJ, 100, 604
- Chung, A., van Gorkom, J. H., Kenney, J. D. P., & Vollmer, Bernd, 2007, ApJ, 659, L115
- Dale, D. A. et al. 2005, ApJ, 633, 857

- de Jong, T., Klein, U., Wielebinski, R., & Wunderlich, E., 1985, *A&A*, 147, L6
- Dickman, R. L., Snell, R. & Schloerb, F. P. 1985, *ApJ*, 309, 326
- Draine, B. T. et al. 2007, *ApJ*, 663, 866
- Dunne, L., Eales, S., Edmunds, M., Ivison, R., Alexander, P., & Clements, D. L., 2000, *MNRAS*, 315, 115
- Engelbracht, C. W. et al., 2007 *PASP*, 119, 994
- Fumagalli, M. & Gavazzi, G., 2008, *A&A*, 490, 571
- García-Burillo, S., Combes, F., Schinnerer, E., Boone, F., & Hunt, L. K. 2005, *A&A*, 441, 1011
- García-Burillo, S., et al., 2008, *A&A*, submitted (ArXiv:08104892v1)
- Gao, Y. & Solomon, P. M., 2004, *ApJ*, 606, 271
- Gavazzi, G., Boselli, A., Pedotti, P., Gallazzi, A., & Carrasco, L. 2002, *A&A*, 396, 449
- Gavazzi, G., et al., 2003, *A&A*, 400, 451
- Gavazzi, G., et al., 2008, *A&A*, 482, 43
- Giovanelli, R., et al., 2005, *AJ*, 130, 2598
- Giovanelli, R., et al., 2005, *AJ*, 133, 2569
- Gordon, K. D., Engelbracht, C. W., Rieke, G. H., Misselt, K. A., Smith, J.-D. T., & Kennicutt, R. C. 2008, *ApJ*, 682, 336
- Greve, T. R., et al. 2005, *MNRAS*, 359, 1165
- Hafok, H., & Stutzki, J., 2003, *A&A*, 398, 959
- Haynes, M. P., Giovanelli, R., & Kent, B. R. 2007, *ApJ*, 665, L19
- Helfer, T. T., Thornley, M. D., Regan, M. W., Wong, T., Sheth, K., Vogel, S. N., Blitz, L, & Bock, D. C.-J. 2003, *ApJS*, 145, 259
- Ho, L. C., Filippenko, A. V., & Sargent, W. L. W. 1997, *ApJS*, 112, 315
- Iono, D. et al. 2008, *ApJ*, submitted

- Israel, F. P., 2008, A&A, in press (ArXiv:811.4058v1)
- Israel, F. P., 2009, in preparation.
- Jogee, S., Scoville, N., & Kenney, J. D. P., ApJ, 630, 837
- Kenney, J. D. P. & Young, J. S., 1986, ApJ, 301, L13
- Kenney, J. D. & Young, J. S., 1988, ApJS, 66, 261
- Kenney, J. D. & Young, J. S., 1988b, ApJ, 326, 588
- Kenney, J. D. P. & Young, J. S., 1989, ApJ, 344, 171
- Kenney, J. D. P., Wong, O. I., Abranson, A. , Howell, J. H., Murphy, E. J., & Helou, G. X., 2008, in “The Evolving ISM in the Milky Way & Nearby Galaxies” (arXiv:0803.2532)
- Kennicutt, R. C. 1998, ApJ, 498, 541
- Kennicutt, R. C. et al. 2003, PASP, 115, 928
- Kennicutt, R. C. et al. 2007, ApJ, 671, 333
- Knapen, J. H., Beckman, J. E., Cepa, J., van der Hulst, T., & Rand, R. J. 1992, ApJ, 385, L37
- Knapen, J. H., Cepa, J., Beckman, J. E., Soledad del Rio, M., & Pedlar, A. 1993, ApJ, 416, 563
- Knapen, J. H., Beckman, J. E., Shlosman, I., Peletier, R. F., Heller, C. H., & de Jong, R. S. 1995, ApJ, 443, L73
- Knapen, J. H., Beckman, J. E., Heller, C. H., Shlosman, I., & de Jong, R. S. 1995, ApJ, 454, 623
- Knapen, J. H., Beckman, J. E., Cepa, J., & Nakai, N. 1996, A&A, 308, 27
- Komugi S., Kohno, K., Tosaki, T., Nakanishi, H., Onodera, S., Egusa, F., & Sofue, Y. 2007, PASJ, 59, 55
- Koopman, R. A., Kenney, J. D. P., & Young, J. S. 2001, ApJS, 135, 125
- Koopmann, R. A. & Kenney, J. D. P. 2004a, ApJ, 613, 866
- Koopmann, R. A. & Kenney, J. D. P. 2004b, ApJ, 613, 851

- Kuno, N. et al. 2007, PASJ, 59, 117
- Laine, S., Shlosman, I., Knapen, J. H., & Peletier, R. F. 2002, ApJ, 567, 97
- Larson, R. B., Tinsley, B. M., & Caldwell, C. N. 1980, ApJ, 237, 692
- Leroy, A. K., Walter, F., Brinks, E., Bigiel, F., de Blok, W. J. G., Madore, B., & Thornley, M. D., 2008, AJ, in press (ArXiv0810.2556v1)
- Maloney, P. & Black, J. 1988, ApJ, 325, 389
- Mauersberger, R., Henkel, C., Walsh, W., & Schulz, A., 1999, ApJ, 341, 256
- Mei, S., et al. 2007, ApJ, 655, 144
- McLaughlin, D. E., 1999, ApJ, 512, L9
- Murphy, E. J., Kenney, J. D. P., Helou, G. X., Chung, A., & Howell, J. H. 2008, in “The Evolving ISM in the Milky Way & Nearby Galaxies” (ArXiv: 0802.2281)
- Nakanishi, H. et al. 2006, ApJ, 651, 804
- Paturel, G., Petit, C., Prugniel, Ph., Theureau, G., Rousseau, J., Brouty, M., Dubois, P., & Cambresy, L. 2003, A&A, 412, 45
- Petitpas & Wilson, 2000, ApJ, 538, L117
- Prescott, M. et al., 2007, ApJ, 668, 182
- Rosolowsky, E., & Blitz, L. 2005 ApJ, 623, 826
- Sakamoto, K., Okumura, S. K., Ishizuki, S., & Scoville, N. Z., 1999, ApJS, 124, 403
- SINGS Team, 2006, Spitzer Infrared Nearby Galaxies Survey Fourth Data Delivery User’s Guide, SSC, Pasadena
- Sofue, Y., Koda, J., Nakanishi, H., & Onodera, S., 2003, PASJ, 55, 17
- Sofue, Y., Koda, J., Nakanishi, H., & Onodera, S., 2003, PASJ, 55, 59
- Stark, A. A., Knapp, G. R., Bally, J., Wilson, R. W., Penzias, A. A., & Rowe, H. E., 1986, ApJ, 310, 660
- Strong, A. W., et al. 1988, A&A, 207, 1
- Thornley, M. D. & Wilson, C. D., 1994, ApJ, 421, 458

- Vogel, S., Kulkarni, S., & Scoville, N., 1988, *Nature*, 334, 402
- Vollmer, B., Balkowski, C., Cayatte, V., van Driel, W., & Huchtmeier, W., 2004, *A&A*, 419, 35
- Warren, B. E. et al., 2009, in preparation
- Williams, J. P., de Geus, E. J., & Blitz, L. 1994, *ApJ*, 428, 693
- Wilson, C. D. & Walker, C. E. 1994, *ApJ*, 432, 148
- Wilson, C. D., Walker, C. E., & Thornley, M. D. 1997, *ApJ*, 483, 210
- Wilson, C. D., Howe, J. E., & Balogh, M. L. 1999, *ApJ*, 517, 174
- Yao, L., Seaquist, E. R., Kuno, N., & Dunne, L., 2003, *ApJ*, 588, 771
- Young, L. M., Bendo, G. J., & Lucero, D. M., 2009, *AJ*, in press (arXiv:0811.1381v1)
- Young, J. S. & Scoville, N. Z. 1991, *ARA&A*, 29, 581
- Young, J. S., et al., 1995, *ApJS*, 98, 219

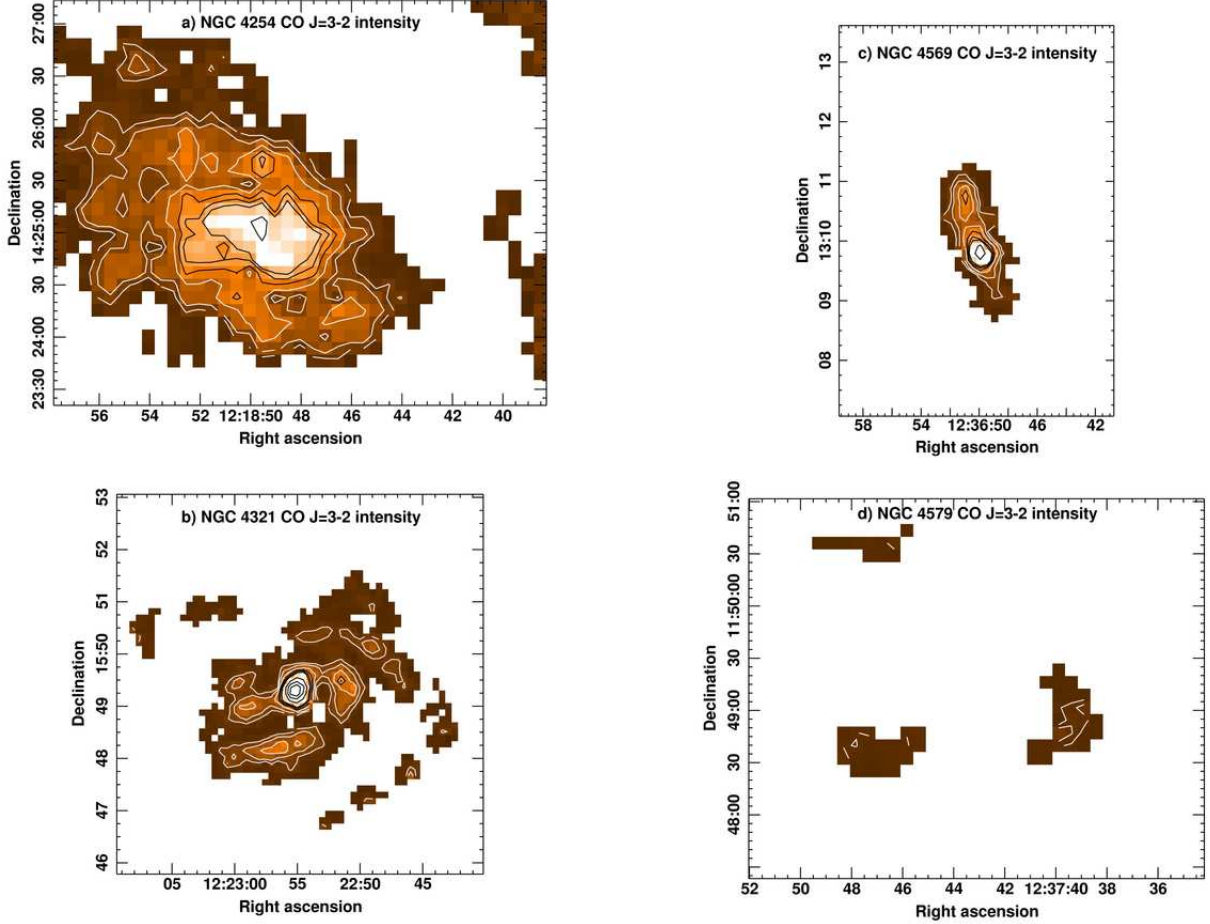


Fig. 1.— (a) CO $J=3-2$ integrated intensity for NGC 4254. Contours are 1,2,4,6,8,10,20 K km s^{-1} and greyscale runs from -3 to 15 K km s^{-1} . Coordinate epoch is J2000. (b) CO $J=3-2$ integrated intensity for NGC 4321. Contours are 1,2,4,6,8,10,20,30,40,50 K km s^{-1} and greyscale runs from -3 to 15 K km s^{-1} . (c) CO $J=3-2$ integrated intensity for NGC 4569. Contours are 1,2,4,6,8,10,20 K km s^{-1} and greyscale runs from -3 to 15 K km s^{-1} . (d) CO $J=3-2$ integrated intensity for NGC 4579. Contours are 0.25,0.5 K km s^{-1} and greyscale runs from -3 to 15 K km s^{-1} .

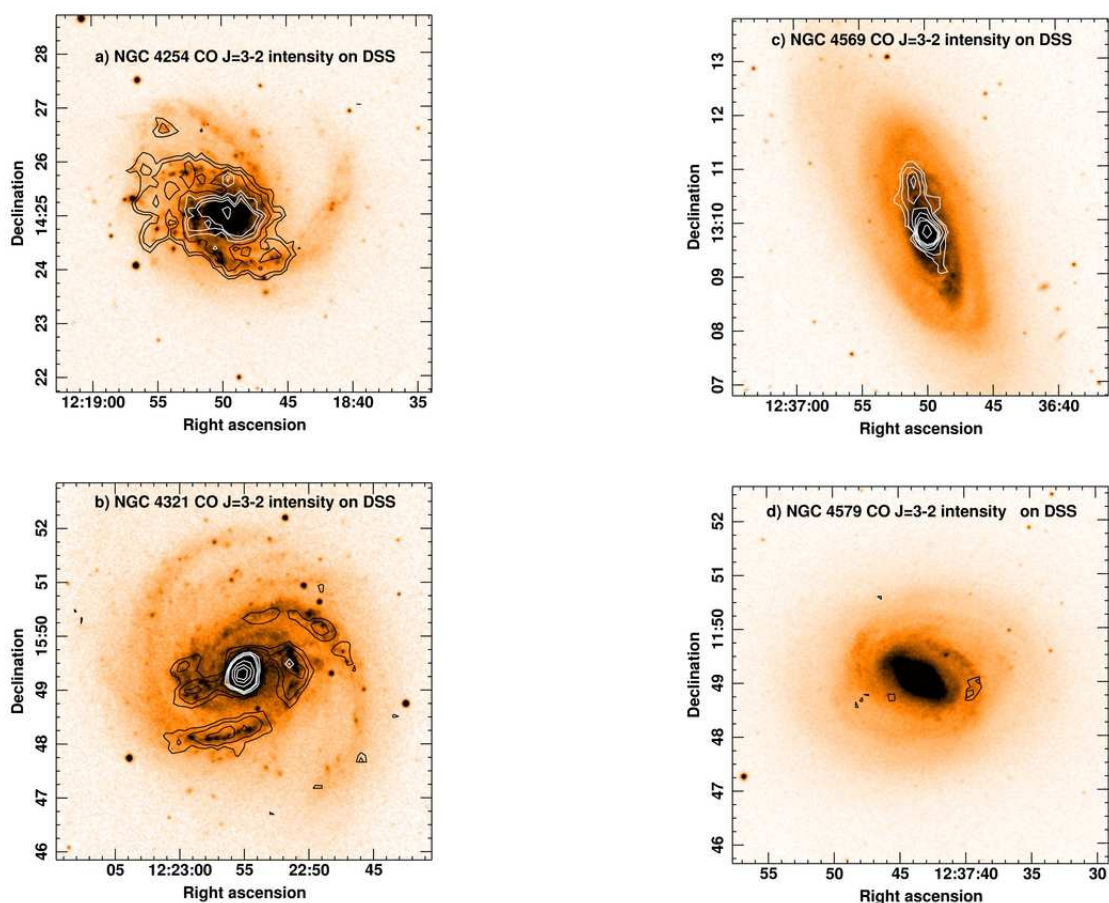


Fig. 2.— (a) CO $J=3-2$ integrated intensity for NGC 4254 overlaid on an image from the Digitized Sky Survey. Contours are 1,2,4,6,8,10,20 K km s^{-1} . Coordinate epoch is J2000. (b) CO $J=3-2$ integrated intensity for NGC 4321 overlaid on an image from the Digitized Sky Survey. Contours are 1,2,4,6,8,10,20,30,40,50 K km s^{-1} . (c) CO $J=3-2$ integrated intensity for NGC 4569 overlaid on an image from the Digitized Sky Survey. Contours are 1,2,4,6,8,10,20 K km s^{-1} . (d) CO $J=3-2$ integrated intensity for NGC 4579 overlaid on an image from the Digitized Sky Survey. Contours are 0.25,0.5 K km s^{-1} .

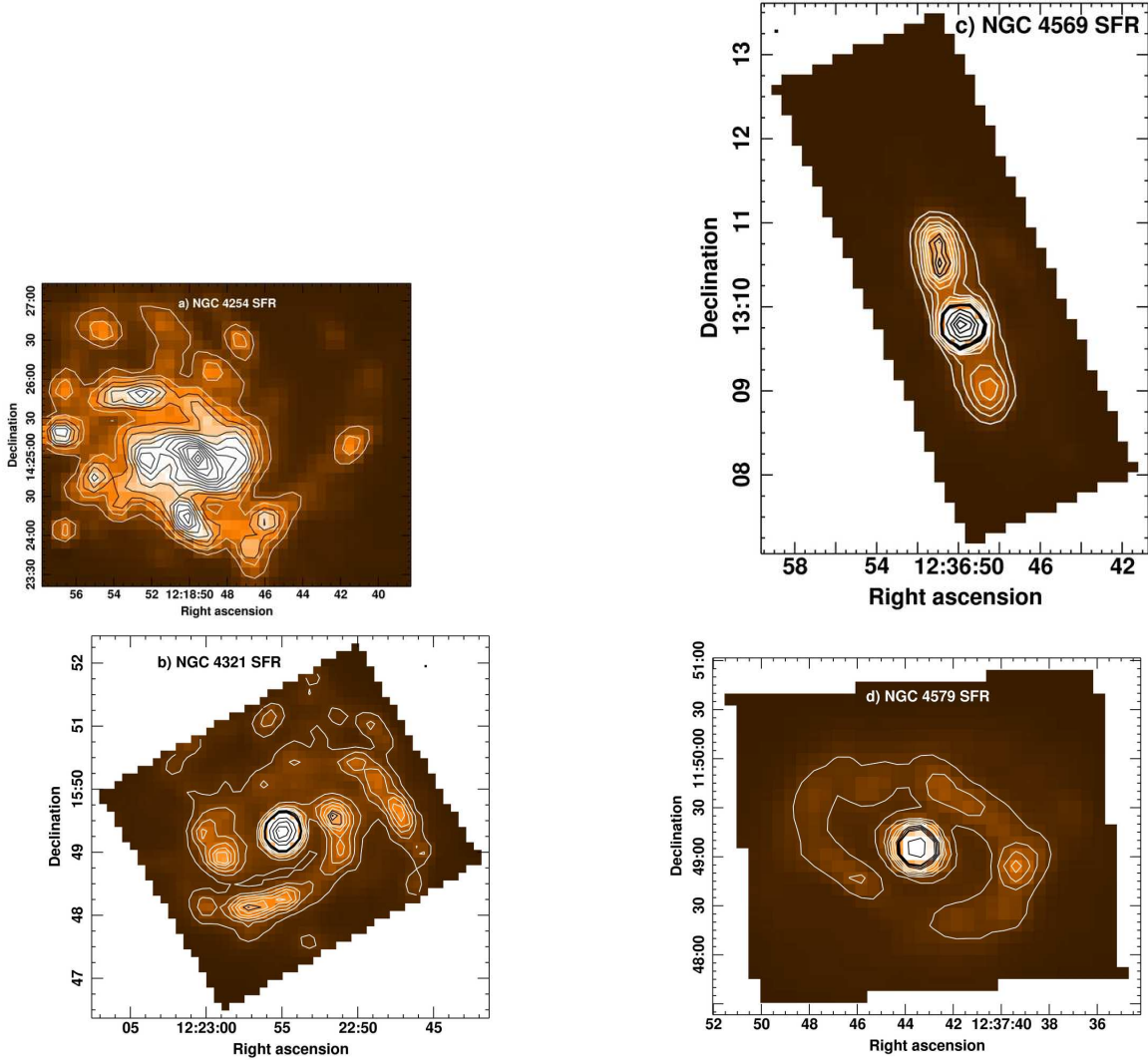


Fig. 3.— (a) Star formation rate surface density for NGC 4254. Contours are 8 to 120 by 8 in units of $10^{-3} M_{\odot} \text{ yr}^{-1} \text{ kpc}^{-2}$ and greyscale runs from -6 to $48 \times 10^{-3} M_{\odot} \text{ yr}^{-1} \text{ kpc}^{-2}$. Coordinate epoch is J2000. (b) Star formation rate surface density for NGC4321. Contours are 4 to 40 by 4 and then 40 to 200 by 40 in units of $10^{-3} M_{\odot} \text{ yr}^{-1} \text{ kpc}^{-2}$ and greyscale runs from -6 to $48 \times 10^{-3} M_{\odot} \text{ yr}^{-1} \text{ kpc}^{-2}$. (c) Star formation rate surface density for NGC4569. Contours are 4 to 40 by 4 and then 40 to 200 by 40 in units of $10^{-3} M_{\odot} \text{ yr}^{-1} \text{ kpc}^{-2}$ and greyscale runs from -6 to $48 \times 10^{-3} M_{\odot} \text{ yr}^{-1} \text{ kpc}^{-2}$. (d) Star formation rate surface density for NGC4579. Contours are 4 to 40 by 4 and then 40 to 80 by 40 in units of $10^{-3} M_{\odot} \text{ yr}^{-1} \text{ kpc}^{-2}$ and greyscale runs from -6 to $48 \times 10^{-3} M_{\odot} \text{ yr}^{-1} \text{ kpc}^{-2}$. Note that the central AGN may dominate the emission in NGC 4579 and so this image does not provide an accurate measure of the star formation rate in the central region of this galaxy.

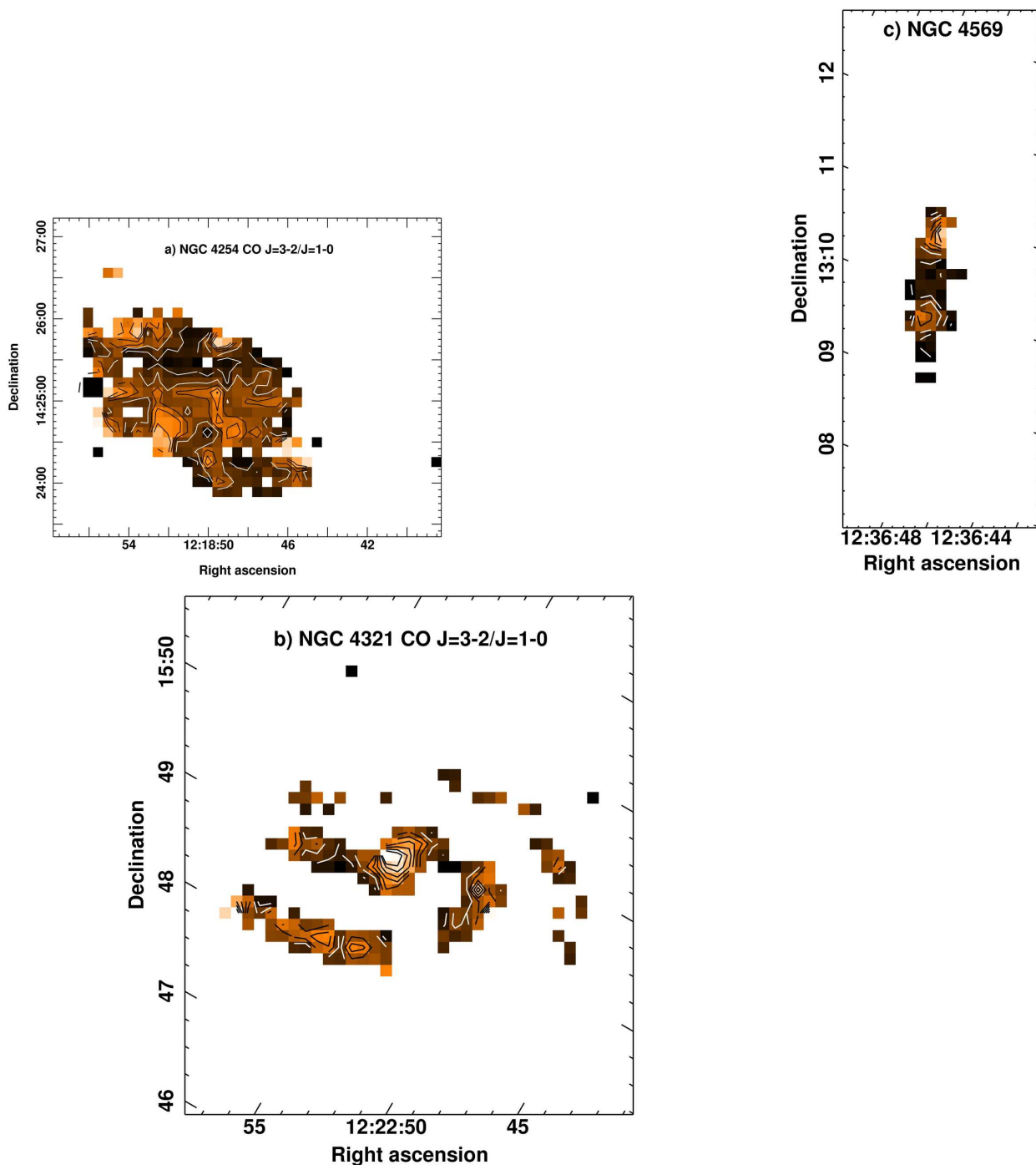


Fig. 4.— (a) CO $J=3-2/J=1-0$ ratio for NGC4254. Contours are 0.2,0.3 (white), 0.4 to 0.7 by 0.1 (black) and greyscale runs from 0.1 to 1 with lighter colors corresponding to higher values. Coordinate epoch is J2000. (b) CO $J=3-2/J=1-0$ ratio for NGC4321. Contours are 0.2,0.3 (white), 0.4 to 0.9 by 0.1 (black) and greyscale runs from 0.1 to 1. Note that this map is oriented at an angle of 30 degrees. (c) CO $J=3-2/J=1-0$ ratio for NGC4569. Contours are 0.1,0.2,0.3 (white), 0.4 to 0.7 by 0.1 (black) and greyscale runs from 0.1 to 1. Note that this map is oriented at an angle of 23 degrees.

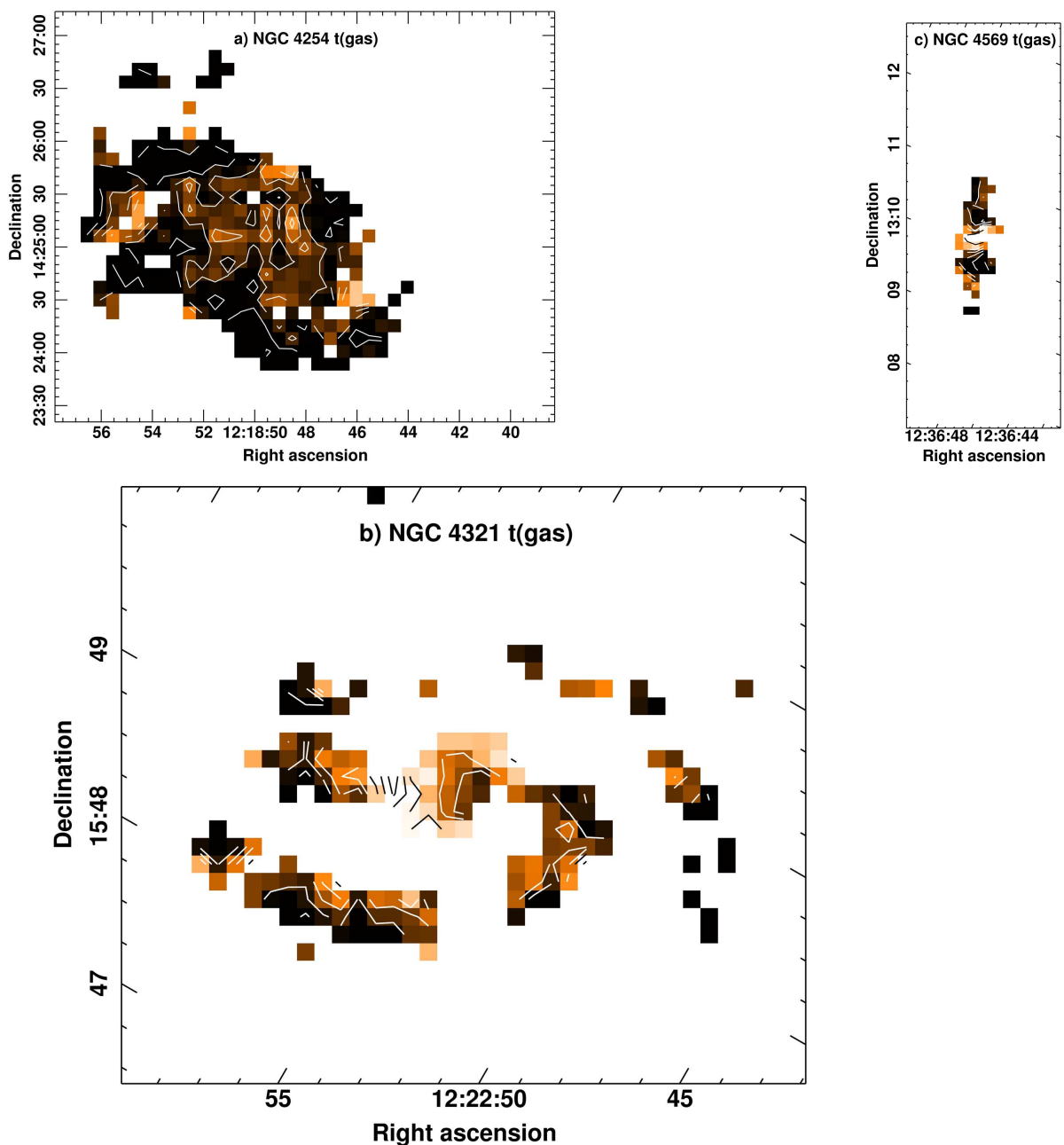


Fig. 5.— (a) Gas depletion time calculated from the CO $J=3-2$ intensity for NGC4254. Contours are 0.8 to 2.0 Gyr by 0.4 Gyr and greyscale runs from 1 to 3 Gyr with lighter colors corresponding to higher values. (b) Gas depletion time calculated from the CO $J=3-2$ intensity for NGC4321. Contours are 0.8 to 2.0 Gyr by 0.4 Gyr (white), 3, 4.5, 6 Gyr (black) and greyscale runs from 1 to 3 Gyr Note that this map is oriented at an angle of 30 degrees. (c) Gas depletion time calculated from the CO $J=3-2$ intensity for NGC4569. Contours are 0.8 to 2.0 Gyr by 0.4 Gyr (white) and 3 Gyr (black) and greyscale runs from 1 to 3 Gyr Note that this map is oriented at an angle of 23 degrees.

Table 1. Galaxy Properties

Galaxy	RA(2000) (hms)	Dec(2000) ($^{\circ}$ $'$ $''$)	V_{hel} (km s^{-1})	Type ^a	D_{25} ^a ($'$)	i ^a ($^{\circ}$)	B_T ^a (mag)	$\log F_{H\alpha}$ ^b ($\text{erg s}^{-1} \text{cm}^{-2}$)	HI mass ^c ($10^9 M_{\odot}$)	HI deficiency ^b
NGC 4254	12:18:49.6	14:24:59	2412	Sa(s)c	5.4	29	10.44	-10.95	4.7	0.02
NGC 4321	12:22:54.9	15:49:20	1599	SAB(s)bc	7.6	32	10.05	-11.13	2.5	0.52
NGC 4569	12:36:49.8	13:09:46	-179	SAB(rs)ab	10.4	63	10.26	-11.83	0.82	0.99
NGC 4579	12:37:43.5	11:49:05	1540	SAB(rs)ab	5.6	37	10.48	-11.54	0.74	1.00

^aFrom Buta et al. (2007)

^bFrom Koopman et al. (2001).

^cFrom Kenney & Young (1989), adjusted to a distance of 16.7 Mpc.

Table 2. Observational Parameters

Galaxy	ΔX ^a ($''$)	ΔY ^a ($''$)	PA ^a ($^{\circ}$)	Date ^b	\overline{T}_{sys} (K)	$\overline{\tau}$ ^c (225 GHz)	t_{int} ^d (s)	ΔT ^e (mK)	resolution ($''$)
NGC 4254	162	138	0	0214,0228,0427	472	0.10-0.16	90	14	14.5
NGC 4321	228	186	30	0211,0213	318	0.04-0.12	30	15	14.5
NGC 4569	312	138	23	0212,0213	380	0.07-0.12	40	15	14.5
NGC 4579	168	132	95	0228,0301	373	0.06-0.12	60	13	14.5

^aSize and orientation of mapped region.

^bMonth,day; all observations done in 2008.

^cRange of atmospheric optical depth at 225 GHz on dates when data were obtained.

^dTypical integration time per point in the map.

^eRms noise in spectra at 20 km s^{-1} resolution on T_A^* scale; divide by 0.67 for T_{MB} .

Table 3. CO $J=3-2/J=1-0$ line ratios

Region	NGC 4254	NGC 4321	NGC 4569	NGC 4579
Global	0.33 ± 0.15^a	0.36 ± 0.19	0.25 ± 0.16	...
Central ^b	0.43 ± 0.11	0.79 ± 0.21	0.34 ± 0.11	...
Bar ends	...	0.42 ± 0.16	0.53 ± 0.18^c	...
	...	0.36 ± 0.12	0.06 ± 0.03	...
Disk peaks	...	0.41 ± 0.12	...	0.15 ± 0.05
	...	0.31 ± 0.10

^aAverage value \pm Standard deviation

^bThe line ratio measured over the central 8-9 pixels.

^cThe northern half of NGC 4569 has the higher line ratio.

Table 4. Molecular gas masses

Galaxy	SFR ^a (M _⊙ yr ⁻¹)	$L_{CO}(3-2)$ (10 ⁸ K km s ⁻¹ pc ²)	M_{H_2} ^b ($R=0.6$) (10 ⁹ M _⊙)	M_{H_2} ^c ($R=0.34$) (10 ⁹ M _⊙)	M_{H_2} ^d (Kuno) (10 ⁹ M _⊙)	M_{H_2} ^e (Helfer) (10 ⁹ M _⊙)
NGC 4254	4.8	5.6	3.0	5.3	6.5	...
NGC 4321	2.7	3.7	2.0	3.5	3.1	6.50
NGC 4569	1.1	1.3	0.67	1.2	3.0	2.40
NGC 4579	<0.9	<0.19	<0.10	<0.18	1.4	...

^aTotal star formation rate derived from H α and 24 μ m images shown in Figure 3 and described in §2. Note that the true central star formation rate may be overestimated if nuclear activity contributes substantially to the 24 μ m flux; this is certainly the case in NGC 4579.

^bMass of molecular hydrogen gas calculated from the CO $J=3-2$ luminosity and assuming a CO $J=3-2/1-0$ line ratio of $R=0.6$; see §3 for details.

^cMass of molecular hydrogen gas calculated from the CO $J=3-2$ luminosity using the measured average CO $J=3-2/1-0$ line ratio of $R=0.34$; see §3 for details.

^dMass of molecular hydrogen gas measured from the CO $J=1-0$ images from Kuno et al. (2007) and using the CO-to-H₂ conversion factor (2×10^{20} cm⁻² (K km s⁻¹)⁻¹) and distance (16.7 Mpc) adopted in this paper.

^eMass of molecular hydrogen gas from Helfer et al. (2003) measured from the CO $J=1-0$ line using the NRAO 12m telescope, adjusted to a distance of 16.7 Mpc.

Table 5. Gas depletion times (Gyr)

Region	NGC 4254	NGC 4321	NGC 4569	NGC 4579
CO $J=3-2$				
Global	1.11±0.02(0.42) ^a	1.70±0.07(0.94)	1.6±0.1(0.9)	...
Central ^b	1.31±0.07(0.25)	2.2±0.2(0.7)	0.92±0.08(0.25)	...
Disk peaks	...	1.3-1.6	0.60±0.01(0.01),1.22±0.07(0.22) ^c	0.25±0.08
CO $J=1-0$				
Global	2.13±0.08(1.32)	3.3±0.2(2.2)	5.4±0.6(4.1)	...
Central ^b	2.1±0.2(0.6)	2.0±0.3(1.0)	1.8±0.2(0.7)	...
Disk peaks	...	2.1-2.5	2.0±0.3(1.0),9.0±0.6(0.8) ^d	...

^aAverage value ± uncertainty in the mean (standard deviation)

^bThe line ratio measured over the central 8-12 pixels.

^cThe northern half of NGC 4569 has the larger gas depletion time.

^dThe southern half of NGC 4569 has the larger gas depletion time.